Contribution from the Department of Chemistry,
Stanford University, Stanford, California 94305

Variable Photon Energy Photoelectron Spectroscopic Studies of Covalent Bonding in $3d^{10}$ Transition-Metal Compounds

Stephen V. Didziulis, Susan L. Cohen, Kristine D. Butcher, and Edward I. Solomon*

Received November 18, 1987

Variable photon energy photoelectron spectroscopy (PES) is used to determine the valence band electronic structure and to study the covalent bonding properties of three tetrahedral, $3d^{10}$ transition-metal complexes with σ-donor, π-donor ligands: ZnO, $ZnCl_4^{2-}$, and CuCl. PES data obtained over the photon energy range of 16.7-1486.6 eV show dramatic intensity changes of valence band features that are caused by changes in photoionization cross sections and resonance effects at the metal 3p absorption edge. Intensity changes with photon energy allow detailed assignments of spectra to be made by using molecular orbital theory. Analyses of the peak intensities and binding energies provide a measure of the covalent bonding. Larger ZnO 3d band splitting relative to that for $ZnCl_4^{2-}$ indicates greater ligand field strength ($10Dq$) for the oxide ligands, which arises from the stronger σ-bonding interactions of the Zn^{2+} 3d with the O^{2-} 2p orbitals. The increased effective nuclear charge on Zn^{2+} shifts the d levels below the ligand levels, making them bonding and reversing the sign of the tetrahedral $10Dq$ value. This greater effective nuclear charge on Zn^{2+} also significantly lowers the energy of the empty metal 4s and 4p levels, resulting in greater covalent stabilization of the ligand bonding levels in $ZnCl_4^{2-}$ than in CuCl. The relative contributions of ionic and covalent bonding in $ZnCl_2$ and CuCl are examined and related to the much greater thermodynamic stability of Zn^{2+} complexes with donor ligands.

I. Introduction

The elucidation of the electronic structure and bonding properties of transition-metal complexes is a fundamental goal in physical inorganic chemistry. Many spectroscopic techniques, particularly optical absorption and electron paramagnetic resonance, have been used to probe the bonding interactions of the d-orbital manifold of transition-metal complexes.[1] These methods, however, require an incompletely filled d subshell. This precludes the study of a very important set of compounds with d^{10} electron configurations. In the first transition series, $3d^{10}$ complexes exist for both Cu(I) and Zn(II) ions, and in this work, the electronic structures of tetrahedral metal ion sites in ZnO, $ZnCl_4^{2-}$, and CuCl are studied with photoelectron spectroscopy (PES), a technique ideally suited for d^{10} systems.

PES is a direct probe of the electronic structure of d^{10} systems as electrons in all levels can be ionized to continuum states, allowing the binding energies of the complete set of valence levels to be determined. Several authors[2,3] have successfully used PES to study gas-phase Zn(II) d^{10} molecules, with crystal field and spin-orbit coupling effects invoked to explain the observed splittings of the Zn 3d orbitals. In addition, solid-state ZnO[4-7] and CuCl[8-15] have been studied with PES, with the goal of understanding the electronic properties and band structures[4,5,14] or the chemisorption behavior of these important materials.[16-19] We have extended this work by exploiting variable photon energy effects on valence band PES spectra of solid ZnO, $ZnCl_4^{2-}$, and CuCl, which enable detailed assignments of valence band features and an experimental analysis of d^{10} electronic structure and bonding interactions.

The effects of varying the input photon energy on PES peak intensities are basically twofold. First, the cross sections of the various valence levels of metal complexes often change in dramatically different ways with changes in photon energy. In particular, metal 3d cross sections show a delayed intensity maximum in the photon energy region of 40-50 eV (30-40 eV above threshold) while both O 2p and Cl 3p cross sections peak near their ionization thresholds before declining with increasing photon energy.[20] The Cl 3p cross section declines precipitously after threshold, going through a local intensity minimum (called a Cooper minimum) near 50 eV photon energy.[21] The second effect of changing photon energy involves resonance at metal absorption edges.[22] At the edge, a metal core level electron (most often from 3p states) is excited to a metal-centered orbital, x in Scheme I. This excited state then decays through a highly allowed Super Coster Kronig (SCK) Auger process involving two d electrons to an ionized final state. For d^{10}, x in Scheme I cannot be a d orbital. This requires the final state achieved by resonance to be a d ionization plus shake-up state, enhancing a satellite peak. The SCK decay mechanism is highly allowed as the transitions occur among orbitals with the same principal quantum number and the metal 3d electrons have large repulsive interactions facilitating the Auger process. The binding energy position of the satellite and its resonance behavior can provide information about the metal d electron Coulomb repulsion present in the complex (as in Hubbard theory[23-25]) and the nature of x in Scheme I.

Scheme I

$$\text{absorption} \quad 3p^6 3d^n \rightarrow 3p^5 3d^n x^1$$

$$\text{SCK Auger decay} \quad 3p^5 3d^n x^1 \rightarrow 3p^6 3d^{n-2} x^1$$

In ref 26, these variable photon energy effects are described in more detail and used to study the electronic structure of d^9 $CuCl_4^{2-}$ complexes with both D_{4h} and D_{2d} geometries. The valence band peak intensity changes with photon energy in combination with theoretical atomic photoionization cross sections are used both qualitatively to assign spectral features and quantitatively

(1) Solomon, E. I. *Comments Inorg. Chem.* **1984**, *3*, 225 and references therein.
(2) Orchard, A. F.; Richardson, N. V. *J. Electron Spectrosc. Relat. Phenom.* **1975**, *6*, 61.
(3) Bancroft, G. M.; Creber, D. K.; Ratner, M. A.; Moskowitz, J. W.; Topiol, S. *Chem. Phys. Lett.* **1977**, *50*, 233.
(4) Zwicker, G.; Jacobi, K. *Solid State Commun.* **1985**, *54*, 701.
(5) Gopel, W.; Pollman, J.; Ivanov, I.; Reihl, B. *Phys. Rev. B: Condens. Matter* **1982**, *26*, 3144.
(6) Ranke, W. *Solid State Commun.* **1976**, *19*, 685.
(7) Powell, R. A.; Spicer, W. E.; McManamin, J. C. *Phys. Rev. B: Solid State* **1972**, *6*, 3056.
(8) Ishii, T.; Kono, S.; Matsukawa, T.; Sagawa, T.; Kobayasi, J. *J. Electron Spectrosc. Relat. Phenom.* **1974**, *5*, 559.
(9) van der Laan, G.; Sawatzky, G. A.; Haas, C.; Myron, H. W. *Phys. Rev. B: Condens. Matter* **1979**, *20*, 4287.
(10) Westphal, D.; Goldman, A. *J. Phys. C* **1982**, *15*, 6661.
(11) Westphal, D.; Goldman, A. *Solid State Commun.* **1980**, *35*, 441.
(12) Pong, W.; Okada, S. K. *Phys. Rev. B: Condens. Matter* **1979**, *20*, 5400.
(13) Kono, S.; Kobayasi, T. *Solid State Commun.* **1974**, *15*, 1421.
(14) Goldman, A.; Tejeda, J.; Shevchik, N. J.; Cardona, M. *Phys. Rev. B: Solid State* **1974**, *10*, 4388.
(15) Kono, H.; Ishii, T.; Sagawa, T.; Kobayasi, T. *Phys. Rev. Lett.* **1972**, *28*, 1385.
(16) Gay, R. R.; Nodine, M. H.; Solomon, E. I.; Henrich, V. E.; Zeiger, H. J. *J. Am. Chem. Soc.* **1980**, *102*, 6752.
(17) Sayers, M. J.; McClellan, M. R.; Gay, R. R.; Solomon, E. I.; McFeely, F. R. *Chem. Phys. Lett.* **1980**, *75*, 575.
(18) McClellan, M. R.; Trenary, M.; Shinn, N. D.; Sayers, M. J.; D'Amico, K. L.; Solomon, E. I.; McFeely, F. R. *J. Chem. Phys.* **1981**, *74*, 4726.
(19) Zwicker, G.; Jacobi, K. *Surf. Sci.* **1983**, *131*, 179.
(20) Yeh, J. J.; Lindau, I. *At. Data Nucl. Data Tables* **1985**, *32*, 1.
(21) Cooper, J. W. *Phys. Rev.* **1962**, *128*, 681.
(22) Davis, L. C. *Phys. Rev. B: Condens. Matter* **1982**, *25*, 2912.
(23) Hubbard, J. *Proc. R. Soc. London, Ser. A* **1963**, *276*, 238.
(24) Hubbard, J. *Proc. R. Soc. London, Ser. A* **1964**, *277*, 237.
(25) Hubbard, J. *Proc. R. Soc. London, Ser. A* **1968**, *281*, 401.
(26) Didziulis, S. V.; Cohen, S. L.; Gewirth, A. A.; Solomon, E. I. *J. Am. Chem. Soc.* **1988**, *110*, 250.

0020-1669/88/1327-2238$01.50/0

to determine initial-state mixing coefficients with the Gelius model (vide infra). These methods give mixing coefficients for the $CuCl_4^{2-}$ complexes averaged over the d manifold of 75–80% Cu 3d character. The paper also probes the changes in electronic structure occurring on ionization. Significant out-of-resonance intensity of the valence region shake-up transition and the resonance behavior of the PES peaks show that large changes in the initial-state wave functions occur on ionization, requiring a final-state analysis of the PES spectra. Both SCF–Xα–SW calculations and configuration interaction analyses of the PES data show that the initial-state wave functions of predominantly metal d character become predominantly ligand in character upon ionization. This means that ionization of the lowest energy d electrons from the $3d^9$ initial state (a process that corresponds to oxidation of the complex) results in a final state with mainly $d^9\underline{L}$ (one-hole metal, one-hole ligand) and $d^{10}\underline{L}^2$ (two-hole ligand) character. The implications of this on the redox properties of Cu(II) complexes are also discussed.

In this work, we extend the d^9 PES study to examine the electronic structure and bonding of three tetrahedral d^{10} complexes with a systematic variation in both ligands and metal ion. First, the valence band spectra of ZnO are contrasted with those of $ZnCl_4^{2-}$ to determine the effects of changing ligands on the PES band shapes, particularly the metal d band, and the differences in bonding implied by these spectral changes. Next, $ZnCl_4^{2-}$ is compared to CuCl to examine the differences in bonding on changing the d^{10} metal ion in the tetrahedral site. It should be emphasized that this study focuses on the simplest case where bonding interactions involve only σ-donor and π-donor ligands.

The PES methods used to study these $3d^{10}$ complexes follow those of our earlier $3d^9$ work. We apply the cross section dependence on the input photon energy to assign valence band features and quantify the mixing through the Gelius analysis of the peak intensities. The energy splittings of peaks are analyzed in conjunction with a simple molecular orbital model. In particular, the splitting of the 3d photoemission peak in the spectra gives the ligand field splitting ($10Dq$) and the cross sections provide information about the σ and π contributions to $10Dq$. With the d levels and their ligand complements completely filled in d^{10} complexes, any interactions of the metal d orbitals with the ligand p levels will result in no net covalent bonding. This fact makes a study of the ligand levels interacting with the empty metal 4s and 4p orbitals very important, as any covalent bonding must occur through these interactions. The variable photon energy PES study of the ligand levels, therefore, should provide information on the covalent bonding present in these complexes, usually considered to be dominantly ionic. The discussion then considers the thermodynamic properties of Zn(II) and Cu(I) complexes with the goal of understanding covalent contributions to the significantly greater stability of Zn(II) complexes with donor ligands in both solids and solutions.

The materials studied are interesting in their own right, and an understanding of their electronic structure and bonding characteristics has implications in many areas of chemistry and materials science. These metal sites are important as models for catalytic active sites in heterogeneous, homogeneous, and biological systems. Zinc oxide and copper-promoted zinc oxide catalysts are active in methanol synthesis and water-gas shift chemistry, where both Zn(II) and Cu(I) sites appear to be important for catalytic activity.[27] Several metalloenzymes involve Cu ion active sites, and the Cu(I)/Cu(II) redox couple is one of the most important in biological systems. ZnO and CuCl are also semiconductors, making knowledge of their electronic structure of interest, while CuCl has also attracted some attention for its superconducting properties.[28]

II. Experimental Section

The ZnO samples were single crystals grown from the vapor phase with oriented (0001) and (10$\bar{1}$0) surfaces of the wurtzite unit cell prepared by aligning the samples to within 1° by Laue backscattering and then cutting a ~1 mm thick slice with a wire saw. The samples were polished with alumina grit down to 0.5 μm until no pits were observed with optical microscopy and then etched with a 5% HCl solution. Cleaning under ultrahigh vacuum (UHV) was performed by a series of sputter/anneal cycles. Successively lower Ar ion accelerating potentials were used to sputter the surfaces at 1000, 500, and 250 V while the samples were heated at 450 °C. Sample cleanliness was checked with Auger spectroscopy (2 keV, 0.5 μA electron beam), and sputter cycles were repeated until no surface contamination was detected (<1% C, S, Cl). The samples were then annealed two additional times to 450 °C, and the surface order was checked by low-energy electron diffraction (LEED).

Large (25 mm^2), single-crystal Rb_2ZnCl_4 samples were grown from a stoichiometric aqueous solution of $ZnCl_2$ and RbCl. The $ZnCl_4^{2-}$ units exist as isolated molecular ions with nearly tetrahedral geometry in the orthorhombic crystals of space group *Pnam*.[29,30] Samples were mounted with UHV-compatible silver epoxy (EPO TEK H21) and cleaned under a nitrogen environment by polishing with 9 μm grit plastic lapping sheets. After transfer to UHV under N_2, further sample cleaning was performed by grinding with 100 μm grit diamond particles embedded in a nickel wheel or by Ar ion sputtering at 500 V for 5 min. The cleanliness of the samples was checked by core level XPS (C 1s, O 1s) or by the ability to obtain satisfactory valence band spectra at low photon energies, where the cross sections for valence levels of common contaminants are very high. The samples were considered to be clean when the general shape and resolution of the spectra were comparable at low and high photon energies after accounting for changes in cross sections of the $ZnCl_4^{2-}$ features.

The CuCl sample used was a large polycrystal (20 × 5 × 2 mm) of the zinc blende material, and initial sample cleaning was performed by polishing under a nitrogen atmosphere with lapping sheets. Further cleaning was performed as necessary in UHV by Ar ion sputtering at 500 V[31] or by mechanical polishing with the diamond wheel. As with the $ZnCl_4^{2-}$ samples, surface cleanliness was monitored with core level XPS or by the resolution of valence band features at low photon energies.

PES data were obtained on two different instruments, one using conventional radiation sources (a Vacuum Generators [VG] ESCALAB Mk II) and the other employing synchrotron radiation (Perkin-Elmer PHI system). The ESCALAB contains a rare-gas discharge lamp that was operated with both He (21.2, 40.8, and 48.4 eV) and Ne (16.7 and 26.8 eV) as well as a twin-anode X-ray source (Mg Kα, 1253.6 eV; Al Kα, 1486.6 eV). The system has been described elsewhere,[26] although it is important to note that the ESCALAB uses a hemispherical electron energy analyzer with a fairly small 6° cone of acceptance, which allows angular effects to be observed with single-crystal surfaces. All ESCALAB spectra were obtained at normal emission unless otherwise stated. The discharge lamp is located at an angle of 65°, and the X-ray anodes (run at 100 W) are at 45° relative to the analyzer. The analyzer pass energy was kept at 5 eV for the intense photon lines (He I and Ne I) and at 20 eV for all other photon energies. Base pressures of better than 5×10^{-11} Torr were regularly achieved; the pressure rose to $\sim 2 \times 10^{-10}$ Torr during operation with the discharge lamp.

Photoelectron spectra at photon energies other than those listed above were obtained with synchrotron radiation from the Grasshopper monochromator on SPEAR beam line III-1 at the Stanford Synchrotron Radiation Laboratory (SSRL) under both dedicated and parasitic conditions. Variable inlet and exit slits on the monochromator allowed a constant photon energy resolution of 200 meV to be maintained.[32-34] In addition, beam line transmission filters that minimize higher order contributions to the monochromatized radiation[33,34] were used up to 70 eV (the filters lose effectiveness and are less essential at higher photon energies). The UHV system used was a Perkin-Elmer PHI system with a double-pass cylindrical mirror analyzer (CMA) and a base pressure better than 1×10^{-10} Torr. The system has been described elsewhere.[26] Synchrotron radiation entered the chamber at an angle of 85° relative to the central axis of the analyzer, and all samples were rotated by 10–15° to accept more light and eliminate the possibility of light impinging on the sample holders. The pass energy for all synchrotron PES spectra was maintained at 25 eV.

(27) Klier, K. *Appl. Surf. Sci.* **1984**, *19*, 267 and references therein.
(28) Chu, C. W.; Rusakov, A. P.; Huang, S.; Early, S.; Geballe, T. H.; Huang, C. Y. *Phys. Rev. B: Condens. Matter* **1978**, *18*, 2116.
(29) McGinnety, J. A. *Inorg. Chem.* **1974**, *13*, 1057.
(30) Brehler, B. *Z. Kristallogr.* **1957**, *109*, 68.
(31) Care was taken to ensure that Ar ion sputtering did not reduce the Cu(I) ions. This was monitored by the position and shape of the X-ray-induced $L_3M_{4,5}M_{4,5}$ Auger peak.
(32) Brown, F. C.; Bachrach, R. Z.; Lien, N. *Nucl. Instrum. Methods* **1978**, *152*, 73.
(33) Stohr, J. *Instruction Manual for the New Grasshopper Monochromator*; Stanford Synchrotron Radiation Laboratory: Stanford, CA, 1980.
(34) Pate, B. B. Ph.D. Thesis, Stanford University, 1984.

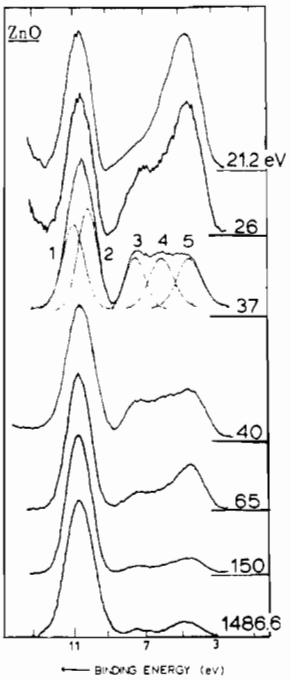

Figure 1. Variable photon energy valence band PES data of ZnO.

Resonance PES data were collected at SSRL by tuning the radiation near the metal 3p absorption edge, ~90 eV for Zn(II) and ~76 eV for Cu(I). Constant initial state (CIS) spectra of the valence band features were obtained by simultaneously scanning the photon energy and analyzed kinetic energy such that the intensity profile of a peak at constant binding energy is obtained. In these spectra, the beam line slits were adjusted such that the photon energy resolution was always better than 200 meV and the analyzer pass energy was increased to 50 eV to increase the signal intensity. Constant final state (CFS) spectra are absorption edges collected with partial yield detection.[35,36] The photon energy was scanned while electrons in the secondary tail at a kinetic energy of 8.0 eV were analyzed. The beam line slits and pass energy were set as with the CIS scans.

All spectra were signal-averaged until sufficient signal to noise had been established. For PES data, the semiconducting ZnO and CuCl samples normally needed only 10–20 scans at one photon energy. The insulating $ZnCl_4^{2-}$ samples required a charge-neutralizing electron flood gun to obtain spectra. The flood gun energy (0–2.0 eV) and current at the sample (10–100 nA) were adjusted until the energy position of the valence band features did not shift with time. Data for $ZnCl_4^{2-}$ were collected in sets of 10 scans, which were then added together after compensting for any kinetic energy shifts that occur with time due to differential charging from changing radiation intensity or flood gun instability. All data taken at SSRL were normalized to the incident photon flux by a monitor consisting of a stainless steel or nickel mesh located in the path of the monochromatized radiation and a total yield channeltron detector. The number of photoelectrons emitted by the mesh is proportional to the photon flux;[37] this signal was collected simultaneously with the spectra and used to normalize the data.

Standard versions of the Xα–SW code were used to calculate the molecular orbital energy levels and wave functions of a $CuCl_4^{3-}$ cluster. The α values of Schwarz[38] and l values of 5, 5, and 3 for the outer, copper, and chloride spheres, respectively, were used for the tetrahedral molecular ion with Cu–Cl bond lengths of 2.34 Å. The Norman criteria[39] were used to determine the sphere radii (2.72 bohr for Cu^+ and 2.596 bohr for Cl^-).

III. Results

(A) ZnO. Variable photon energy valence band PES spectra of ZnO over the range of 21.2–1486.6 eV (Figure 1) show two sets of peaks, one centered at 10.7-eV binding energy and the second between 4 and 8 eV. The deeper binding energy feature becomes more intense relative to the lower energy peaks with increasing photon energy, allowing the assignment of the deeper binding energy peak as arising from Zn 3d photoemission and the lower binding energy features as ionization from O 2p states by comparison to atomic subshell photoionization cross sections.[20] This assignment is consistent with previous work.[7]

Closer examination of spectra at selected photon energies shows a complex splitting pattern with peaks exhibiting interesting intensity changes with photon energy. First, our highest resolution data of the (0001) d band at 21.2 eV (Figure 2a) shows a pronounced shoulder on the high-binding-energy side of the peak with a splitting of 0.7–0.8 eV. The intensity of the shoulder depends on the angle of detection (the angle of incident radiation also changes as the sample is rotated). Further, angle integrated spectra taken in the photon energy range of 37–65 eV with synchrotron radiation (Figure 1) show that at least three peaks are present in the oxide band, with approximate binding energies of 7.5, 6.0, and 4.5 eV. Spectra at all photon energies were fit with five Gaussian/Lorentzian peaks (labeled 1 and 2 in the d band and 3–5 in the oxide band in Figure 1) by an iterative peak fitting

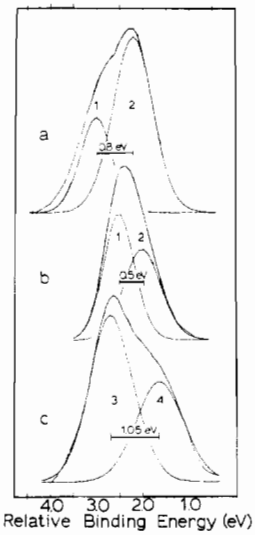

Figure 2. Comparison of the PES d bands of the three complexes: (a) ZnO at 21.2 eV; (b) $ZnCl_4^{2-}$ at 40.8 eV; (c) CuCl at 21.2 eV.

Table I. Binding Energies (eV), Listed with Spectrometer E_F = 0 eV for ZnO and CuCl[a]

	ref to Zn $2p_{3/2}$		ref to Cl $2p_{3/2}$	
	ZnO	$ZnCl_4^{2-}$	CuCl	$ZnCl_4^{2-}$
M $2p_{3/2}$	1021.70	1021.70	932.35	1022.35
M $2p_{1/2}$	1044.70	1044.80	952.25	1045.45
Cl $2p_{3/2}$		198.00	198.65	198.65
Cl $2p_{1/2}$		199.40	200.20	200.05
M $3p_{3/2}$	88.60	88.70	74.40	89.45
M $3p_{1/2}$	91.20	91.30	76.80	91.95
$3d^84s^1$ satellite	31.70	32.40	15.70	33.05
M 3d				
	11.10 [1 (t_2)]	10.55 [1 (t_2)]	1.70 [4]	11.20 [4]
	10.30 [2 (e)]	10.05 [2 (e)]	2.75 [3]	10.70 [3]
ligand valence p				
		7.60 [3a]		8.25 [3a]
	7.30 [3]	5.80 [3b]	6.65 [1]	6.45 [3b]
	5.90 [4]	4.80 [4]	5.35 [2]	5.45 [4]
	3.50 [5]	3.90 [5]		4.55 [5]
3p → 4s	89.0	90.3	76.9	90.3
	91.6	93.1	78.9	93.1
metal 4s	+0.4	+1.5–1.8	+2.5	+0.85–1.15

[a] Values listed for metal 4s levels are above E_F and are given as +. Peak numbers are shown in brackets.

(35) Stohr, J.; Jaeger, R.; Brennan, S. *Surf. Sci.* **1982**, *117*, 503.
(36) Hecht, M. Ph.D. Thesis, Stanford University, 1982.
(37) Lindau, I.; Spicer, W. E. In *Synchrotron Radiation Research*; Winick, H., Doniach, S., Eds.; Plenum: New York, 1980.
(38) Schwarz, K. *Phys. Rev. B: Solid State* **1972**, *5*, 2266.
(39) Norman, J. G., Jr *Mol. Phys.* **1976**, *31*, 1191.

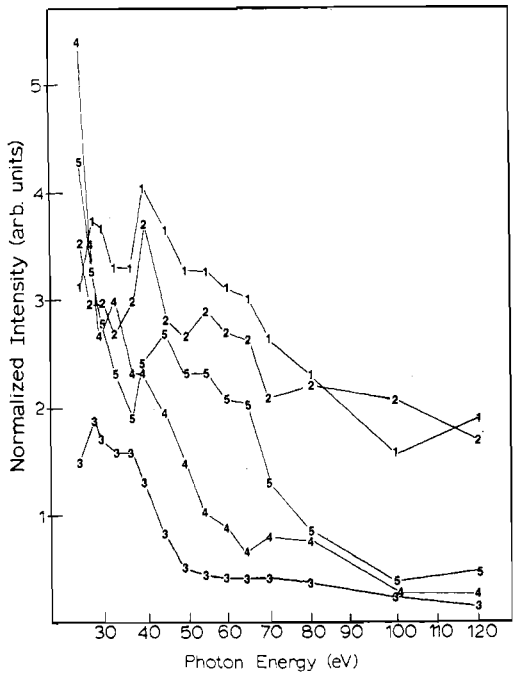

Figure 3. Absolute integrated intensities of peaks 1–5 from the fits of the angle integrated synchrotron spectra of ZnO. Beam line transmission filter changes at 37 and 70 eV lead to discontinuities in the intensity plots.

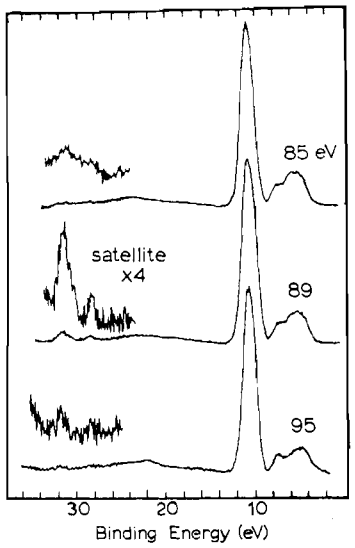

Figure 4. Valence band PES of ZnO taken before the Zn 3p edge at 85 eV, at the Zn 3p → 4s transition energy of 89 eV, and after the edge at 95 eV.

procedure that varied the peak position, Lorentzian peak width, and peak height to minimize the χ^2 difference between the fit and the spectrum after a linear background had been subtracted. These fits gave consistent splittings of 0.8 eV in the d band, 1.5 eV between peaks 3 and 4, and 1.4 eV between peaks 4 and 5. The binding energies of these valence levels and selected core levels as determined by XPS are given in Table I.

The absolute integrated intensity profiles of the five peaks from the fits of all synchrotron data are shown in Figure 3 (the changes in analyzer transmission function and electron escape depth with changing electron kinetic energy have not been accounted for). Peaks 1 and 2 show delayed intensity maxima near 40 eV, which confirms their assignment as Zn 3d photoemission. Peak 4 starts very high in intensity and drops rapidly with increasing photon energy as expected for ionization from pure O 2p levels. Peaks 3 and 5, however, display important differences from the atomic O 2p cross section. Peak 5 starts very intense and shows an initial decrease before going through a relative maximum in the 40–50-eV region, indicating that this peak has a mixture of O 2p and

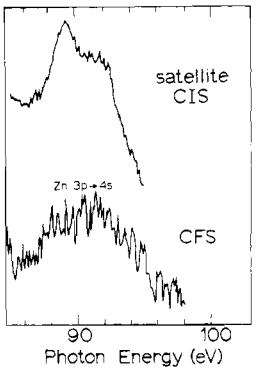

Figure 5. Comparison of the ZnO satellite CIS intensity profile to the CFS edge data.

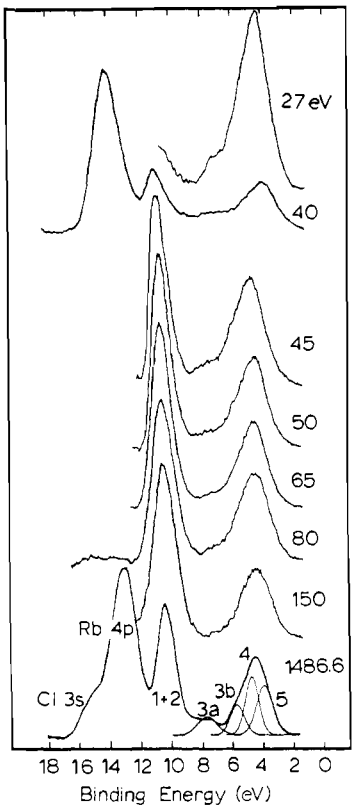

Figure 6. Variable photon energy PES data of Rb_2ZnCl_4. The spectra taken at 40, 80, and 1253.6 eV are extended to show the Cl 3s and Rb 4p ionization.

Zn 3d photoionization character. In the synchrotron data in Figure 3, peak 3 is less intense than peaks 4 and 5 at low photon energies, has nearly the same intensity as peaks 4 and 5 at 37 eV, and decays with peaks 4 and 5 at higher photon energies. The 21.2-eV spectrum in Figure 1 shows that peak 3 has very little intensity relative to the rest of the oxide band. This pattern is characteristic of the Zn 4s cross section,[40] which displays a Cooper minimum in the photon energy range of 15–22 eV.[20]

As the photon energy is increased from 85 to 89 eV in Figure 4, a satellite peak becomes evident at a binding energy of 31.7 eV[41] while the d-band intensity decreases by 11%. The CFS data

(40) The theoretical atomic subshell photoionization cross sections of ref 20 predict the metal 4s cross section to be 20–30 times smaller than those of the metal 3d which would make its influence on the valence band peak intensities insignificant. However, experimental results on atomic Cu show that σ_{4s} has about the same magnitude as σ_{3d} in the photon energy region cnsidered here, indicating that it would, in fact, make an important contribution to the valence band spectrum as we observe. See: Dyke, J. M.; Fayad, N. K.; Morris, A.; Trickle, I. R. *J. Phys. B* **1979**, *12*, 2985.

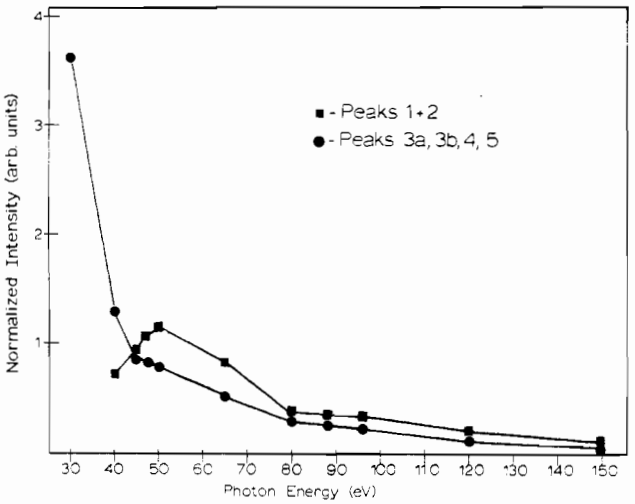

Figure 7. Absolute intensity profiles of the $ZnCl_4^{2-}$ features determined by peak area measurement of the synchrotron spectra.

in Figure 5 provide the absorpiton spectrum at the Zn 3p → 4s edge, indicating that this transition occurs from ~88 to 93 eV. The satellite CIS intensity profile (Figure 5) shows two maxima at photon energies of 89.0 and 91.6 eV which correlate to the broad absorption feature in the CFS data, indicating that the satellite is in resonance with the edge transition. The 2.6-eV splitting of the satellite CIS is attributed to the spin–orbit splitting of the Zn 3p hole. The satellite has roughly 5% of the d-band intensity at 89 eV.

(B) $ZnCl_4^{2-}$. Valence band spectra of $ZnCl_4^{2-}$ obtained at several photon energies are shown in Figure 6. Photoemission from the counterion (Rb^+) can be assigned immediately from the intensity changes in the peak at 13.5-eV binding energy. The peak is very intense at 40 eV and decreases by a factor of about 100 at 80 eV, leading to its assignment as the Rb 4p levels as theoretical cross sections predict this large change.[20] The remaining features at binding energies of ~16, 10.3, and 8–3 eV arise from ionization from the $ZnCl_4^{2-}$ species. The 16-eV peak is the Cl 3s level, determined by comparison to spectra of $CuCl_4^{2-}$ complexes.[26]

Peak 1+2 at 10.3 eV is visible only at photon energies above 35 eV in Figure 6, as the large Rb 4p peak obscures it at lower photon energies. Peak 1+2 shows a delayed maximum near 50 eV in the integrated intensity plots of Figure 7 and occurs at a binding energy similar to that of the Zn 3d band in ZnO, leading to its assignment as ionization from the Zn d band. As shown in the high-resolution data in Figure 2b, no splitting can be resolved in the $ZnCl_4^{2-}$ d band and the peak is only approximately 0.7 times as broad as that of ZnO (e.g., at 40 eV, ZnO has a fwhm of 1.75 eV; the fwhm is 1.20 eV for $ZnCl_4^{2-}$). As with ZnO, two peaks (labeled 1 and 2 in Figure 2b) were used to fit the d band, producing features at binding energies of 10.55 and 10.05 eV.

The lower binding energy set of valence band peaks in Figure 6 is very intense at low photon energies and decreases rapidly as the photon energy increases (Figure 7), demonstrating the assignment of these levels as the Cl 3p valence levels, which have a Cooper minimum in their atomic cross section near 50 eV. While the ligand band clearly shows a well-resolved, small peak (3a) at 7.6 eV in Figure 6, the dominant intensity at low energy is broad and somewhat featureless relative to that in the ZnO spectra in Figure 1.

Our highest resolution data of the Cl band taken at 21.2 and 48.4 eV (Figure 8b,c) reveal at least three features near 7.6, 6.0, and 4.7 eV. It proved impossible to fit spectra at all photon energies with only three peaks in the Cl band as this constraint

(41) Two satellite peaks are evident for all the samples studied, and the deeper binding energy, more intense peak is labeled as the satellite. The presence of more than one peak is attributed to the multiplets of the $3d^8 4s^1$ final state, with the two features usually attributed to the ^2G and ^4F states of the metal ion.

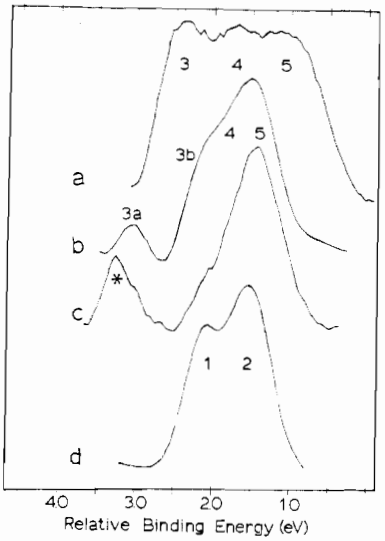

Figure 8. Comparison of the PES ligand bands of the d^{10} complexes: (a) ZnO at 37 eV; (b) $ZnCl_4^{2-}$ at 21.2 eV; (c) $ZnCl_4^{2-}$ at 48.4 eV; (d) CuCl at 21.2 eV. The apparent shift in peak 3a in spectra b and c is due to an additional photon line at 51 eV exciting the Zn 3d band (*).

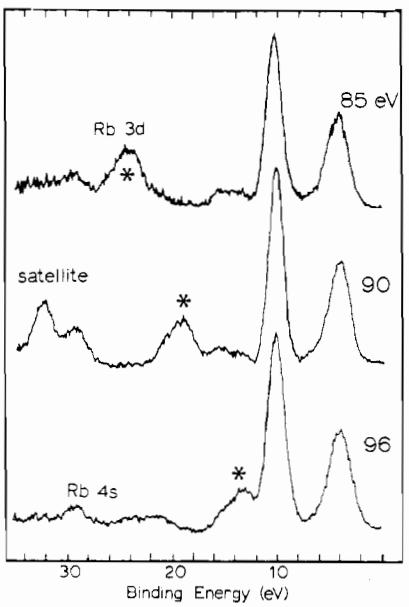

Figure 9. Resonance PES data for $ZnCl_4^{2-}$ taken before the Zn 3p edge at 85 eV, at the 90-eV 3p → 4s transition energy, and after the edge at 96 eV. The peak moving to lower binding energy with increasing photon energy arises from the ionization of the Rb 3d levels with second-order radiation (*).

required significant changes in the binding energies and widths of these peaks to obtain satisfactory fits at different photon energies. The Cl band, therefore, was fit with four peaks as labeled in Figures 6 and 8b, giving the following binding energies: peak 3a, 7.6 eV; peak 3b, 5.8 eV; peak 4, 4.8 eV; peak 5, 3.9 eV. The overlap of peaks 3b, 4, and 5 still prevented the generation of a meaningful intensity plot similar to that obtained for ZnO in Figure 3. Binding energies listed in this paragraph and in Table I are obtained by referencing the valence band peaks in the XPS spectrum to the binding energy of the Zn $2p_{3/2}$ core level. This core level in the insulating sample is assumed to have the same binding energy as the $2p_{3/2}$ level in ZnO.

Resonance PES data for $ZnCl_4^{2-}$ are presented in Figure 9. The satellite peak again has little intensity out of resonance but becomes evident in the 90-eV spectrum at a binding energy of 32.4 eV. The CIS satellite intensity profile in Figure 10 shows intensity maxima at photon energies of 90.3 and 93.1 eV, coincident with the features in the CFS edge spectrum. The satellite peak has ~20% of the d-band intensity at 90.3 eV. A CIS scan

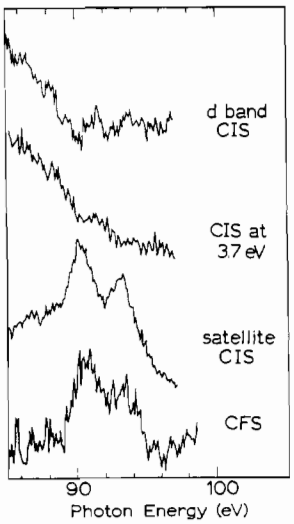

Figure 10. CIS intensity profiles of the $ZnCl_4^{2-}$ d band, the top edge of the Cl band, and the intense, deeper binding energy satellite. The CFS edge spectrum is included to show the energy position of the Zn 3p → 4s transition.

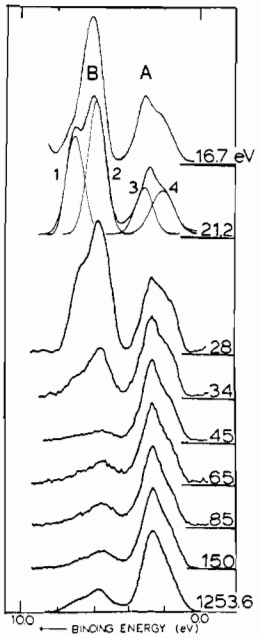

Figure 11. Variable photon energy valence band PES data of CuCl.

of the Zn d band through the 3p edge shows two distinct intensity minima at these same photon energies. Finally, a CIS scan taken at the top portion of the Cl band at a binding energy of 3.7 eV shows two very weak minima at 90.3 and 93.1 eV.

(C) CuCl. The variable photon energy PES spectra of CuCl are shown in Figure 11 and have been presented elsewhere.[26] Two principal peaks are evident (A at low binding energy and B at deeper binding energy), each of which is split into two peaks, producing features at binding energies of 1.7, 2.7 eV and of 5.5, 6.8 eV. The dramatic decrease in the relative intensity of peak B as the photon energy is increased to 45 eV identifies peak B as photoionization from the Cl 3p levels and peak A as Cu 3d photoemission. This assignment is consistent with previous work[14,26] and shows that the CuCl d band is above the ligand band in contrast to the case for $ZnCl_4^{2-}$. The synchrotron data were fit with four Gaussian/Lorentzian peaks as shown in Figure 11, and the intensity profiles of peaks 1–4 are presented in Figure 12. The two peak fits of feature B give a 1.3-eV splitting between peaks 1 and 2, and the intensity plots in Figure 12 show that Cl 3p character, with a Cooper minimum near 50 eV, predominates in the peaks. Peak 2, however, retains more intensity through the minimum, indicating that this feature also contains some Cu

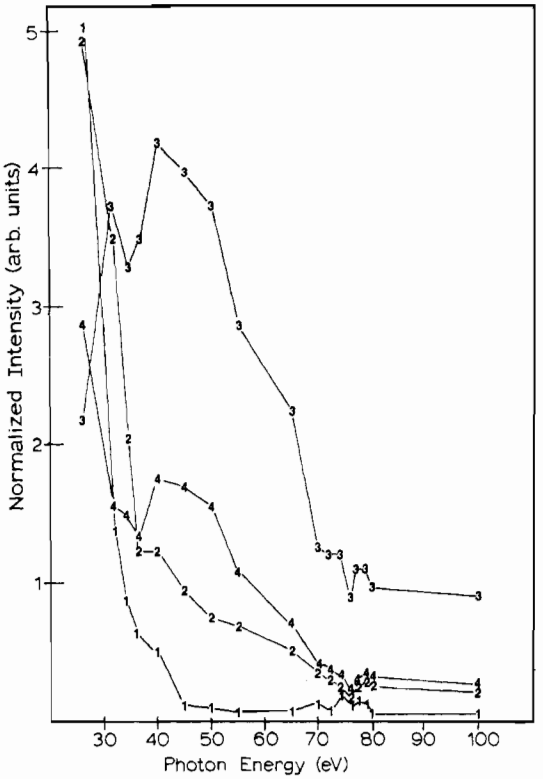

Figure 12. Absolute intensities of CuCl peaks 1–4 as a function of photon energy from the fits of the synchrotron data.

3d character as the 3d cross section has a maximum in intensity near 45–50 eV. The relative intensities of peaks 1 and 2 at very low photon energies are also quite interesting, as peak 1 has little intensity relative to that of peak 2 at 16.7 eV and goes through a relative maximum at 21.2–26 eV (Figure 11). The low intensity of peak 1 at 16.7 eV indicates the presence of 4s character (much the same as peak 3 in the ZnO spectra) as the Cu 4s Cooper minimum occurs at a slightly lower binding energy than the Zn 4s minimum.[20]

The two peak fits of the d band (Figure 2c) give a peak 3–peak 4 splitting of 1.05 eV (0.25 eV smaller than the Cl band splitting) with the two components having distinctively different intensity profiles in Figure 12. Peak 3 clearly shows the delayed intensity maximum of an essentially pure Cu 3d level in the photon energy range of 40–50 eV. Peak 4 also has a delayed local maximum, but only after an intensity decline at lower photon energies, revealing the additional presence the of Cl 3p cross section.

The core level binding energies of CuCl obtained from XPS are given in Table I and are referenced to the spectrometer Fermi level. For comparison to CuCl, the binding energies of the $ZnCl_4^{2-}$ levels have also been referenced to the Cl 2p levels. This method of referencing gives 0.65 eV higher binding energies for $ZnCl_4^{2-}$ than referencing to the Zn 2p levels.[42]

Resonance PES data on CuCl have been presented elsewhere,[26,43] and the results are summarized in Figure 13. First, the satellite appears at a binding energy of 15.6 eV and has very little intensity out of resonance. The satellite CIS intensity profile shows maxima at photon energies of 76.9 and 78.7 eV, in the same photon energy region as the features corresponding to the Cu 3p → 4s transition in the CFS edge spectrum (bottom of Figure 13). The spectrum at the top of Figure 13 was taken at 76.9 eV, where the satellite has 11% of the d-band intensity. A broad intensity minimum is observed in the Cu d band CIS profile in the region of 77–79 eV.

(42) The exact binding energies for the Zn 2p levels in $ZnCl_4^{2-}$ are likely between the two extremes given in Table I. The shift to deeper binding energy from the ZnO core levels relates to a chemical shift from greater effective positive charge on the Zn^{2+} ion in $ZnCl_4^{2-}$.

(43) Ishii, T.; Taniguchi, M.; Kakizaki, A.; Naito, N.; Sagawara, H.; Nagakura, I. *Phys. Rev. B: Condens. Matter* **1986**, *33*, 5664.

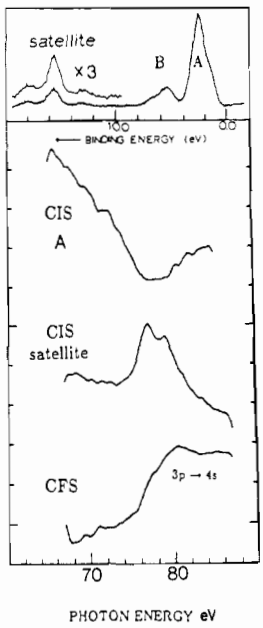

Figure 13. Top: CuCl valence band spectrum taken at 76.9 eV. Bottom: CIS intensity profiles of the Cu d band and the satellite compared to the CFS 3p → 4s edge.

Scheme II

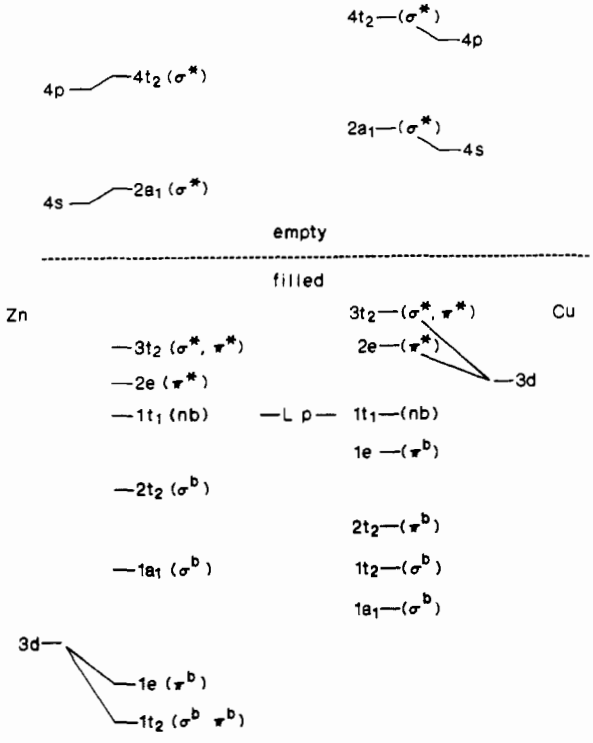

IV. Analysis

(A) PES Peak Assignments and Comparison to Molecular Orbital Calculations. Assignment of the PES spectra and analysis of the bonding interactions occurring in these d^{10} complexes are based on the T_d molecular orbital diagram given in Scheme II for the ML_4 cluster, where the metal d levels are below the ligand valence p levels for Zn^{2+} (left) and above the ligand valence p levels for Cu^+ (right). This relative order of the metal d and ligand p orbitals is based on the PES data presented here and on atomic spectroscopy,[44] which both indicate that the greater effective nuclear charge on the Zn^{2+} ion shifts the d levels below the ligand

(44) Moore, C. E. *Atomic Energy Levels*; U.S. National Bureau of Standards Circular 467; U.S. Government Printing Office: Washington, DC, 1952.

Table II. Xα-SW Calculated Energy Levels (eV) and Wave Functions

(A) ZnO (ZnO_4^{6-})[a]

level	energy	% Zn	% O
$3t_2$	+0.75	26	61
$1t_1$	0.00	0	100
2e	−0.15	23	66
$2t_2$	−1.25	6	65
$1a_1$	−2.30		
1e	−3.65	77	14
$1t_2$	−3.74	77	18

(B) $ZnCl_4^{2-}$[b]

level	energy	% Zn	% Cl
$3t_2$	+0.25	15	79
$1t_1$	0.00		
2e	−0.25	6	80
$2t_2$	−0.90	8	80
$1a_1$	−2.25		
1e	−4.67	94	4
$1t_2$	−4.88	87	13

(C) CuCl ($CuCl_4^{3-}$)

level	energy	% Cu	% Cl
$3t_2$	+3.16	84	11
2e	+2.84	91	5
$1t_1$	0.00	1	83
$2t_2$	−0.47	8	74
1e	−0.57	6	74
$1t_2$	−0.89	15	76
$1a_1$	−1.77	21	71

[a] Taken from ref 47. [b] Taken from ref 50.

levels. In $3d^{10}$ metal oxide and halide complexes, the filled metal d and the empty 4s and 4p levels interact with the filled valence levels of the σ-donor, π-donor chloride and oxide ligands. The tetrahedral ligand field splits the d levels into e and t_2 sets with the magnitude of the splitting reflecting the relative amounts of σ (t_2) and π (e) interaction of the d orbitals with the ligand valence p levels. As stated in the Introduction, the metal d and ligand p levels are full and cannot contribute to the overall covalent bond stabilization of these materials. The σ-bonding interactions of empty metal 4s and 4p orbitals stabilize the a_1 and t_2 ligand levels and it is these interactions that produce net covalent bonding. In the d^{10} complexes, it appears from the PES data (vide infra) that the Zn 4s and 4p orbitals are in a much more favorable position than the unoccupied valence orbitals of Cu.

(1) ZnO. For ZnO, peaks 1 and 2 can be assigned as components of the d band with the 0.8-eV splitting reflecting the t_2–e separation, which is $10Dq$ in ligand field theory. This splitting is much too large to derive from crystal field repulsion[45] or spin–orbit splitting ($\xi = 0.14$ eV)[3] of the $3d^9$ final state and must result from covalency. Correlation of the ZnO d band in Figure 2a to the CuCl d band of Figure 2c indicates a reversed splitting pattern; the variable-energy PES data for CuCl are used in Section IV(A)(3) to assign peaks 3 and 4 in Figure 2c as the e and t_2 levels, respectively. This leads to the assignment of peaks 1 and 2 as the t_2 and e levels, respectively, which is the inverse splitting pattern expected from crystal field perturbations for a tetrahedron but is consistent with strong covalent bonding interactions of the d levels with the oxide 2p levels (vide infra). Note that the intensity ratio in the 21.2-eV data of Figure 2a is not that predicted from level degeneracy (t_2:e ratio should be 3:2) and cannot arise from from contributions of ligand cross section ($\sigma_{2p} > \sigma_{3d}$ at 21.2 eV). While angular effects will contribute to this deviation,[4] the dominant contribution is likely t_2-band dispersion. Band structure calculations including the d levels show the t_2 states to appear to deeper binding energy and to be dispersed over 1.0 eV, which

(45) Figgis, B. N. *Introduction to Ligand Fields*; Interscience: New York 1966; Chapter 2.

would lead to a broad PES feature, while the e states are more localized (<0.4 eV).[46] This sort of behavior is not distinguished by the peak-fitting procedure, causing the t_2 level to have an apparently smaller contribution to the valence band intensity. This order of levels but not the magnitude of splitting is also consistent with Xα–SW calculations in Table II.[47]

The three peaks in the oxide band show dramatically different intensity profiles (Figure 3). Peak 4 shows essentially pure O 2p cross section with changing photon energy and is assigned as ionization from nonbonding O 2p $1t_1$ levels. Peak 5 is destabilized from these nonbonding levels by 1.4 eV and exhibits an intensity profile with mixed O 2p and Zn 3d character. The mixed character and destabilization of peak 5 lead to its assignment as ionization from the antibonding 2e* and $3t_2$* levels from the O 2p–Zn 3d interaction. The Xα calculation predicts the $3t_2$* levels to lie at lowest energy, split by 0.75 eV from the nonbonding levels, but this study represents the first experimental confirmation of d character in the oxide band. Many band structure calculations on ZnO treat the d levels as noninteracting low-lying core levels,[48,49] which is clearly inaccurate.

The dominant contribution to net covalent bonding in ZnO must arise from the stabilization of peak 3 by 1.5 eV relative to the nonbonding levels. The low intensity at 21.2 eV is ascribed to the presence of Zn 4s character arising from the σ-bonding interaction of an O 2p level with the empty Zn 4s level.[6] The intensity of peak 3 at 37-eV photon energy in Figure 1 shows that this peak must contain more than just the $1a_1$ (O 2p–Zn 4s) bonding level, as this level would contribute only about 8% of the total oxide band intensity. The Xα calculation in Table IIA predicts the next deepest level to be the $2t_2$ level stabilized through σ-bonding with the Zn 4p levels. We therefore assign peak 3 as containing ionizations from both the bonding $1a_1$ and $2t_2$ levels of ZnO.

The PES data exhibit a satellite peak at 21.0 eV above the d band, which the CIS and CFS spectra in Figure 5 indicate is in resonance with the Zn 3p → 4s transitions at 89.0 and 91.6 eV. As will be discussed in Section IVD, this allows an assignment of the satellite peak as a $3d^{10} \rightarrow 3d^8 4s^1$ d ionization plus d → s shake-up transition. The binding energies of the spin–orbit split Zn 3p levels are 88.6 and 91.2 eV (Table I), which in conjunction with the 3p → 4s edge transition energies place the Zn 4s based $2a_1$* level about 0.4 eV above the Fermi level and 3.8 eV above the top edge of the valence band. The $2a_1$* position obtained above is reasonable, as the optically measured band gap is 3.4 eV at room temperature with the conduction band having mostly Zn 4s character.[46,49] This treatment ignores any differences in orbital relaxation resulting from transitions to bound states as opposed to ionization, which can be substantial. The Zn 3d–4s splitting in ZnO is thus determined to be 11.1 eV, which is larger than the observed free ion splitting of 9.6–10 eV.[44]

(2) $ZnCl_4^{2-}$. The $ZnCl_4^{2-}$ spectra in Figure 6 have important similarities to and differences from those of ZnO (Figure 1). The overall shape is similar, with the 3d band at 10.3 eV, well separated from the ligand features. The most significant difference in the $ZnCl_4^{2-}$ d band shown in Figure 2b is that it has only about 70% of the width of the ZnO d band and has been fit with two peaks split by 0.5 eV. This decreased splitting is indicative of less ligand p–Zn 3d σ-interaction in $ZnCl_4^{2-}$. Consistent with this smaller Zn 3d–Cl 3p interaction is the fact that little d character is evident in the chloride band in the variable photon energy data (Figure 7). While a smaller d-band splitting is not predicted by the Xα calculations in Table IIB,[50] generally less covalent mixing and smaller splittings in the antibonding ligand levels are. In addition, the Zn 2p–3d splitting is 0.4 eV greater in $ZnCl_4^{2-}$ (see Table I), indicating that the d band is stabilized to a lesser degree by bonding with the chloride ligands.

Although its general shape is similar, the chloride band of $ZnCl_4^{2-}$ in the spectra in Figure 6 does not have the distinct features observed in the ligand band of ZnO (Figure 1) with the exception of the deep binding energy peak 3a. Peak 3a has approximately 6% of the total Cl intensity at 21.2 eV, increases to 10% at 30 eV, decreases to 3% at 47 eV (Cl 3p Cooper minimum), and finally returns to about 10% in the XPS valence band spectrum. The low relative intensity at 21.2 eV reflects the presence of a Zn 4s Cooper minimum while the large decrease at 47 eV indicates that the peak has principally Cl 3p cross section. In parallel with the case for ZnO, peak 3a is assigned as ionization from the Zn 4s stabilized $1a_1$ σ-bonding level. Overall, this peak has much lower intensity than peak 3 in the ZnO spectra and contains approximately the correct relative intensity (8%) to be only the $1a_1$ level. If the peak contained both the a_1 and t_2 bonding levels, as assigned in ZnO, the peak should have about 33% of the total Cl 3p photoemission intensity (see Figure 8a).

Comparing the 21.2- and 48.4-eV spectra (Figure 8b,c), one observes that peak 3b at 5.8 eV drops dramatically in intensity relative to the lower binding energy portion of the band (from 15% to 7%). This intensity pattern suggests that this peak is principally Cl 3p but has about the correct intensity at low photon energies to be the Zn 4p stabilized t_2 bonding level. Consistent with this assignment, the ground-state Xα–SW calculation in Table IIB predicts the $ZnCl_4^{2-}$ $2t_2$ level to be the next lowest in energy and to have a greater splitting from the $1a_1$ level than that predicted for ZnO. This assignment is more reasonable than concluding that the peak contains photoemission from both the $2t_2$ and nonbonding $1t_1$ levels, as these features combined should produce 50% of the Cl intensity at low photon energies. Peaks 4 and 5 retain the majority of the Cl band intensity at the Cl 3p Cooper minimum (48.4-eV spectrum in Figure 8c) and, therefore, must be assigned as containing some 3d cross section and hence the antibonding 2e* and $3t_2$* levels. These peaks must also contain ionization from the nonbonding $1t_1$ levels to complete the assignment. The assignments are supported by the Xα results (Table IIB), which predict a $2t_2$–$1t_1$ splitting of 0.9 eV with the 2e, $1t_1$, and $3t_2$ levels spread over only 0.5 eV. Our best effort at determining the energy positions of these levels comes from the four peak fits to the Cl band regions, which gave the following average binding energies: peak 3a ($1a_1$), 7.6 eV; peak 3b ($2t_2$), 5.8 eV; peak 4 ($1t_1$), 4.8 eV; peak 5 ($2e^*/3t_2^*$), 3.9 eV.

The resonance PES data for $ZnCl_4^{2-}$ are similar to the ZnO data but show quantitative differences. From Figure 9, the dominant shake-up satellite peak in $ZnCl_4^{2-}$ is located at a binding energy of 32.4 eV, split from the d band by 22.1 eV. The satellite CIS intensity profile and CFS edge spectrum in Figure 10 show that the resonance enhancement of the satellite results from the Zn 3p → 4s transition, which occurs at photon energies of 90.3 and 93.1 eV (more than 1 eV greater than in ZnO) and confirm the satellite final state as $3d^8 4s^1$ (vide infra). From the binding energy positions of the Zn 3p levels in Table I, the Zn 4s ($2a_1$*) level can be placed at about 1.6 eV above the spectrometer Fermi level, giving a Zn 3d–4s splitting of 12.0 eV. The intensity minima of the d-band CIS profile show that the satellite gains intensity at the expense of the d-band photoemission. The fact that slight minima are observed in the CIS spectrum at the top edge of the Cl band at 3.7 eV confirms that a small amount of metal d character is present and gives the approximate location of the Cl 3p–Zn 3d antibonding levels.

(3) CuCl. The valence band spectra of CuCl in Figure 11 are quite different from those of $ZnCl_4^{2-}$, primarily becaude the Cu d band (A) is at a much lower binding energy, above the ligand levels as shown in Scheme II (right). The d-band splitting in CuCl is 1.05 eV, with an inverted intensity pattern as compared to that of ZnO (Figure 2a,c). The two peaks used to fit the d band have markedly different intensity profiles in Figure 12. Peak 3 displays the delayed intensity maximum of an essentially pure Cu 3d level while peak 4 loses some of its low photon energy intensity before going through a local intensity maximum between 40 and 50 eV, indicating the presence of both Cu 3d and Cl 3p cross section. Peaks 3 and 4 are thereby assigned as the 2e* and $3t_2$* levels,

(46) Lee, D. H.; Joannopoulos, J. D. *Phys. Rev. B: Condens. Matter* **1981**, *24*, 6899.
(47) Tossell, J. A. *Inorg. Chem.* **1977**, *16*, 2944.
(48) Ivanov, I.; Pollmann, J. *Solid State Commun.* **1980**, *36*, 361.
(49) Ivanov, I.; Pollmann, J. *Phys. Rev. B: Condens. Matter* **1981**, *24*, 7275.
(50) Tossell, J. A.; Vaughan, D. J. *Inorg. Chem.* **1981**, *20*, 3333.

respectively, which arise from metal d–ligand p bonding in a tetrahedral ligand field. In this assignment, the 2e* π-level, at deeper binding energy relative to $3t_2$*, must be considered to be weakly antibonding in nature while the $3t_2$* σ-level is strongly antibonding due to the clear presence of Cl character. We thereby obtain the ligand field ordering of levels t_2 above e for a tetrahedron but with a splitting much larger than that predicted by ligand repulsion. As observed earlier in the split ZnO d band, the intensity pattern of the CuCl metal d band splitting is not consistent with a 2:3 (e:t_2) ratio but angular effects cannot be important here as the CuCl sample is polycrystalline. Alternatively, band structure calculations[51-53] indicate that the e level should be localized (about 0.2 eV wide) while the t_2 states form a band 1.5 eV wide that overlaps the e levels.

The Cl band is split into two peaks separated by 1.3 eV (Figure 8d), a larger splitting than that for the Cu d band. The intensity plots of peaks 1 and 2 in Figure 12 clearly show different changes with increasing photon energy, with peak 2 retaining more of its intensity through the Cl Cooper minimum. This effect leads one to assign peak 2 as containing more Cu 3d character than peak 1. Moreover, peak 1 is relatively weak at 16.7 eV and goes through a maximum near 21.2 eV in Figure 11. The peak 1 intensity pattern is similar to that of peak 3 in the ZnO spectra discussed earlier, which is assigned as containing the metal 4s/4p stabilized ligand $1a_1$ and $1t_2$ bonding levels. The σ-bonding $1t_2$ level should also contain some Cu 3d character, although it is not clearly evident. The Xα–SW calculations on a $CuCl_4^{3-}$ cluster in Table IIC predict these levels to fall at deepest binding energies. Peak 2 can then be assigned as arising from the remaining Cl 3p levels, including the π-bonding $2t_2$ and 1e and the nonbonding $1t_1$ levels. Comparison of the Cl bands of CuCl and $ZnCl_4^{2-}$ at 21.2 eV in parts d and b of Figure 8 shows the similarity of these features with the important exception of the much more deeply stabilized $1a_1$ bonding level in $ZnCl_4^{2-}$ (peak 3a). Finally, it is interesting to note from Table I that if the Cl $2p_{3/2}$ core level binding energies of CuCl and $ZnCl_4^{2-}$ levels are aligned, the Cl 3p nonbonding levels fall at very nearly the same binding energy for both samples, near 5.4 eV relative to the Fermi level and roughly 11.9 eV relative to the vacuum level (with ϕ = 6.5 eV for CuCl). This $1t_1$ binding energy is quite close to the nonbonding $1t_1$ binding energies for gas-phase tetrahedral chlorides (including CCl_4,[54] $SnCl_4$,[54] $TiCl_4$,[55] and VCl_4[55]), which range from 11.7 to 12.2 eV.

The resonance PES data in Figure 13 indicate that the shake-up satellite corresponding to the $3d^84s^1$ final state appears at 12.3 eV above the center of the d band. The satellite CIS and the CFS edge spectrum indicate that the Cu $3p_{3/2,1/2} \rightarrow 4s(2a_1^*)$ transition occurs at 76.9 and 78.9 eV. The measured Cu 3p binding energies of 74.4 and 76.4 eV place the unoccupied $2a_1$* level at 2.5 eV above the Fermi level and 3.2 eV above the top of the valence band. This 3.2 eV is comparable to, although smaller than, the 3.4 eV optically measured band gap at room temperature.[56] The measured Cu 3d–4s splitting is 4.8 eV, which is again larger than the Cu(I) free ion value of 3.0 eV.[44]

(B) PES Peak Intensities. The intensities of peaks in valence band PES spectra can be analyzed to determine metal–ligand mixing coefficients through the use of the Gelius–Siegbahn model.[57,58] The model assumes that the intensity of a molecular orbital is proportional to the sum of the atomic cross sections (σ_{ao})

Scheme III

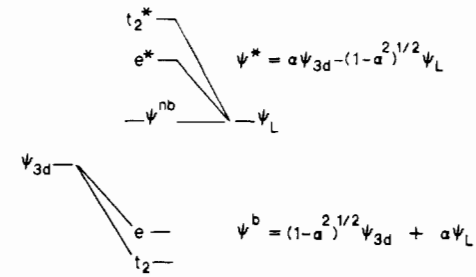

Table III. Mixing Coefficients (α^2) from the Gelius Model

(A) ZnO

photon energy, eV	σ_L[a]	I_{1+2}/I_5	α^2	I_{1+2}/I_{4+5}	α^2
28	5.5	1.74	0.22	0.84	0.16
120	0.24	8.14	0.22	5.34	0.27
1253.6	0.060	17.1	0.15	10.4	0.22

(B) $ZnCl_4^{2-}$

photon energy	σ_L[a]	I_{1+2}/I_{3b+4+5}	α^2
50	0.18	1.80	0.12
80	0.21	1.50	0.15
120	0.18	2.25	0.04
150	0.18	2.15	0.06
1486.6	0.32	1.31	0.05

(C) CuCl

			α^2	
photon energy	σ_L[a]	I_{3+4}/I_2	e + t_2	t_2
16.7	14.7	0.58	0.16	0.27
40	0.13	10.5	0.14	0.24
80	0.21	7.73	0.15	0.25
1253.6	0.31	6.00	0.14	0.24

[a] The relative atomic cross sections for the ligand electrons with σ_d = 1.0 from ref 20.

of its components weighted by their molecular orbital mixing coefficients (c_i):

$$I_{mo} \propto \sum c_i^2 \sigma_{ao} \qquad (1)$$

This expression is most useful when one atomic cross section dominates all others in a particular orbital or at high photon energies (>200 eV) such that cross terms can be neglected.[59] The relative intensities of different peaks in the same valence band spectrum at a given photon energy are used as these photoelectrons will have essentially the same kinetic energy, allowing the analyzer transmission function and electron escape depth contributions to PES peak intensities to be ignored. In this section we focus on the comparison of the d-band intensity to that of its related t_2 and e ligand band counterparts, considering only the relevant parts of the molecular orbital diagram (Scheme III shown for Zn ions). A general equation comparing the intensity of the d band to that of the ligand features is

$$\frac{I_d}{I_L} = \frac{N^d[(1-\alpha^2)\sigma_{3d} + \alpha^2\sigma_L]}{N^L[\alpha^2\sigma_{3d} + (1-\alpha^2)\sigma_L] + N^{nb}\sigma_L} \qquad (2)$$

where N^d is the number of d electrons present, N^L is the number of ligand electrons participating in the bonding interaction with the d band, N^{nb} is the number of ligand nonbonding electrons being considered in the analysis, and σ is the theoretical atomic photoionization cross section for the metal 3d (σ_{3d}) or ligand valence (σ_L) electrons. The relative peak intensities will thus produce mixing coefficients averaged over the d manifold of states.

(1) ZnO. In the application of the Gelius model to the PES spectra of ZnO, the sum of intensities of peaks 1 and 2 (e and t_2 levels of the d band) is compared to that of peak 5 (assigned as the e* and t_2* ionizations). We also consider an alternative

(51) Kleinman, L.; Medwick, K. *Phys. Rev. B: Condens. Matter* **1979**, *20*, 2487.
(52) Zunger, A.; Cohen, M. L. *Phys. Rev. B: Condens. Matter* **1979**, *20*, 1189.
(53) Lewonczuk, S.; Gross, J. G.; Ringeissen, J.; Khan, M. A.; Riedinger, R. *Phys. Rev. B: Condens. Matter* **1983**, *27*, 1259.
(54) Egdell, R. G.; Fragala, I. L.; Orchard, A. F. *J. Electron Spectrosc. Relat. Phenom.* **1979**, *17*, 267.
(55) Egdell, R. G.; Orchard, A. F.; Lloyd, D. R.; Richardson, N. V. *J. Electron Spectrosc. Relat. Phenom.* **1977**, *12*, 415.
(56) Ringeissen, J.; Nikitine, S. *J. Phys. Colloq. (Orsay, Fr.)* **1967**, *28*, C3-48.
(57) Gelius, U.; Siegbahn, K. *Faraday Discuss. Chem. Soc.* **1972**, *No. 54*, 257.
(58) Gelius, U. In *Electron Spectroscopy*; Shirley, D. A., Ed.; North-Holland: Amsterdam, 1972.
(59) Kono, S.; Kobayasi, T. *Solid State Commun.* **1974**, *15*, 1421.

analysis that includes peak 4 as the nonbonding $1t_1$ level to eliminate any ambiguity in assignments due to the overlap of peaks 4 and 5 in the spectra in Figure 1. For all of these calculations, eq 2 is used with $N^d = 10$ electrons. The number of ligand electrons reflects the correct stoichiometry of the material, requiring a total of 6 oxide 2p electrons for ZnO. Thus, N^L is equal to 2.5 electrons and N^{nb} is 1.5 electrons when peak 4 is included. For ZnO, the Gelius model is most useful at low photon energies, where the oxygen cross section is much greater than the Zn 3d cross section (<30 eV), and at high photon energies, where the reverse is true (>100 eV). The relative cross sections used in these calculations (σ_L in Table III) were taken from the atomic subshell cross sections calculated in ref 20.

The results of the analyses including only peak 5 ($N^{nb} = 0$) at 28, 120, and 1253.6 eV are given in Table IIIA and show an average mixing coefficient of $\alpha^2 = 0.20$. When peak 4 is also included, the results are quite consistent with the first method, giving $\alpha^2 = 0.22$. The consistency of the two methods over a wide range of photon energies lends support to the assignments of peak 4 as containing primarily nonbonding electrons and peak 5 as being the antibonding level ionizations.[60]

(2) $ZnCl_4^{2-}$. A similar approach was used in applying the Gelius model to $ZnCl_4^{2-}$, with the following exceptions: (1) The total number of electrons in the ligand levels is 24 and $N^L = 10$ electrons as $ZnCl_4^{2-}$ exists as isolated molecular ions. (2) The entire Cl band except for the peak 3a has been used in the intensity analysis, and the $1t_1$ and $2t_2$ levels have been included as nonbonding levels, making $N^{nb} = 12$ electrons (Scheme II, left). With chloride ligands, the Gelius model may be applied at very low photon energies (<20 eV), where the relative Cl 3p cross section is much greater than the 3d, as well as at and above the Cl 3p Cooper minimum (>45 eV), where $\sigma_{3d} \gg \sigma_{3p}$. With Rb_2ZnCl_4 samples, however, an accurate determination of the d-band intensity can only be made at photon energies greater than 45 eV due to the overlap of the intense Rb 4p peaks at lower photon energies. The results obtained at various photon energies are presented in Table IIIB. The average ligand *n*p–metal 3d mixing coefficient obtained from the Gelius model is about 8%, much smaller than that observed for ZnO. A smaller mixing coefficient is consistent with the qualitative observations of smaller d-band splitting (Figure 2c) and lack of much obvious d character in the variable photon energy PES of the Cl band. Limited mixing is, however, implied by the Cl band CIS intensity minima at resonance in Figure 10 and the remaining intensity in peaks 4/5 at the Cl 3p Cooper minimum (Figure 8c).

(3) CuCl. The Gelius analysis for CuCl is applicable in the same photon energy regimes as for $ZnCl_4^{2-}$. The low photon energy data (16.7 eV in Figure 11), however, is useful for CuCl as no interference from counterion photoemission exists. In applying the model to CuCl, we will compare the intensities of the complete d band (peaks 3 and 4) with the intensity of peak 2 in the Cl band, which has been assigned as containing the ligand p–metal d bonding 1e and $2t_2$ levels as well as the nonbonding $1t_1$. Two methods of comparing these intensities have been employed. The first considers the average mixing over the entire d band as was done for both Zn complexes (eq 2 with $N^L = 2.5$ electrons and $N^{nb} = 1.5$ electrons), and the second considers only mixing in the $3t_2$ level by treating the 2e set as nonbonding (eq 3). The results for CuCl are listed in Table IIIC. The model

$$\frac{I_{3+4}}{I_2} = \frac{6[(1-\alpha^2)\sigma_d + \alpha^2\sigma_{3p}] + 4\sigma_d}{1.5[\alpha^2\sigma_d + (1-\alpha^2)\sigma_{3p}] + 2.5\sigma_{3p}} \quad (3)$$

gives consistent results over the wide range of photon energies analyzed, with an average mixing over the entire d band of 15% and mixing in the $3t_2$ level alone of 25%. Greater metal d–ligand p mixing is expected for CuCl as compared to that for $ZnCl_4^{2-}$ from the observation of greater d–band splitting (compare parts b and c of Figure 2) and the peak intensity profiles in the Cu complex in Figure 12.

Scheme IV

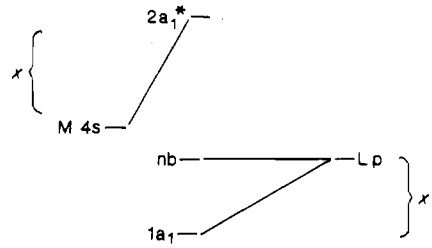

(C) PES Peak Energies. The lack of shake-up peak intensity out of resonance indicates that the effects of final-state relaxation on the nature of the wave functions are limited, and the energy level splittings of the ground-state molecular orbitals of the d^{10} systems can be directly related to the assigned peaks in the PES spectra. Since we have determined the binding energy positions of the ligand nonbonding levels in all three complexes, the energy stabilizations of the ligand bonding a_1 and t_2 levels and, in the case of Zn^{2+}, the destabilizations of the ligand e* and t_2* levels can be obtained in a straightforward manner. As an example, for the ligand p–metal 4s interaction we need consider only the a_1 portion of the molecular orbital diagram of Scheme II, shown in Scheme IV. The energy stabilization of the $1a_1$ level (or destabilization of $2a_1$), x is obtained by solving the secular determinant:

$$\begin{vmatrix} |\text{L p}\rangle & |\text{M 4s}\rangle \\ e_L - E & T \\ T & e_{4s} - E \end{vmatrix} = 0 \quad (4)$$

The bonding interaction matrix element (T) has the form $T = \langle \text{L p}|H|\text{M 4s}\rangle$, and eq 4 produces eigenvalues stabilized and destabilized from their nonbonding positions by

$$x = \frac{(\Delta^2 + 4T^2)^{1/2} - \Delta}{2} \quad (5)$$

where $\Delta = e_L - e_{4s}$ and e_L (e_s) is the energy of the ligand p (metal 4s) orbital prior to interaction. The molecular orbitals produced are simply

$$\Psi(1a_1) = \cos\theta|\text{L p}\rangle + \sin\theta|\text{M 4s}\rangle$$
$$\Psi(2a_1^*) = \sin\theta|\text{L p}\rangle - \cos\theta|\text{M 4s}\rangle \quad (6)$$

where $\tan 2\theta = 2T/\Delta$. The parameters x and Δ can be obtained directly from the PES data, allowing T and the covalent mixing, $\cos^2\theta$, of the wave functions to be obtained. Analogous equations can be written for both the metal 3d–ligand p (e and t_2) and the metal 4p–ligand p (t_2) bonding interactions.

(1) ZnO. This analysis is relatively straightforward for the a_1 levels of ZnO. The value of $x = 1.5$ eV is the peak 3–peak 4 splitting in the PES spectrum in Figure 1, as these features have been assigned as containing the bonding $1a_1$ and the nonbonding $1t_1$ levels, respectively. To determine Δ, we must find the energy of the Zn 4s level prior to the bonding perturbation. Our Zn 3p edge data have placed the perturbed 4s level in ZnO at 0.4 eV above the Fermi level, and if it is assumed that tnis level has been destabilized by the same amount that peak 3 has been lowered in energy from the nonbonding position, then the Zn 4s level prior to bonding (e_{4s}) is at 1.10 eV below E_F. The value of $e_L = 5.90$ eV (Table I) makes Δ equal to 4.8 eV. Values of T and $\cos^2\theta$ obtained from this analysis are given in Table IVA along with the input parameters. The $1a_1$ level is found to have approximately 20% Zn 4s character. The model can be used to study the Zn 4p/O 2p interaction with x also equal to ~1.5 eV, as peak 3 contains both the $1a_1$ and $2t_2$ stabilized levels. The value of Δ

(60) If the intensity of the entire oxide band is used in the Gelius analysis and the $1a_1$ and $2t_2$ levels are included as pure O 2p (i.e. nonbonding), then mixing coefficients of 24% at 28 eV, 25% at 120 eV, and 24% at 1253.6 eV are obtained. This method is obviously an approximation, as it does not include any Zn 4s or 4p contributions but does eliminate any possible error in the assignment of peaks in the oxide band. The fairly close agreement with the other approaches, however, is quite satisfying.

Table IV. Molecular Orbital Model Parameters and Mixing Coefficients

	x, eV	Δ, eV	T	$\cos^2\theta$
		(A) ZnO		
		(1) 2p–3d Levels		
peak 2, e	1.0	−3.4	2.10	0.82
peak 1, t_2	1.8	−3.4	3.06	0.74
		(2) 2p–4s Level		
peak 3, a_1	1.5	4.8	3.11	0.81
		(3) 2p–4p Level		
peak 3, t_2	1.5	11.8	4.47	0.90
		(B) $ZnCl_4^{2-}$		
		(1) 3p–3d Levels		
peak 1, e	0.65	−4.6	1.85	0.89
peak 1, t_2	1.15	−4.6	2.57	0.83
		(2) 3p–4s Level		
peak 2, a_1	2.8	3.7	4.27	0.70
		(3) 3p–4p Level		
peak 3, t_2	1.0	10.7	3.42	0.92
		(C) CuCl		
		(1) 3p–3d Levels		
peak 3, e	0.0	2.8	0.0	1.00
peak 4, t_2	1.05	2.8	2.01	0.79
		(2) 3p–4s Level		
peak 1, a_1	1.30	6.5	3.18	0.86
		(3) 3p–4p Level		
peak 1, t_2	0.30	12.5	1.96	0.95

(the O 2p–Zn 4p splitting) has been estimated from the Zn^{2+} free ion 4s–4p splitting to be 11.8 eV.[44] The results of the calculation for the t_2 level in Table IVA show a larger value of T than that obtained for the a_1 level, but a smaller mixing coefficient (10% Zn 4p).

This treatment can be extended to both the e and t_2 levels of the d band independently, as we have been able to experimentally estimate their splitting. The average stabilization of the d levels is given by the amount of destabilization of the ligand antibonding 2e* and $3t_2$* levels (peak 5 in Figure 1) relative to the nonbonding level $1t_1$ (peak 4 in the spectrum) and has been determined to be 1.4 eV. Since we have concluded that the $1t_2$–1e (peak 1–peak 2) splitting is 0.8 eV for ZnO (Figure 2b), the stabilizations due to bonding are 1.8 eV for $1t_2$ and 1.0 eV for 1e. The value of Δ = 3.4 eV is the same for both levels and is the difference between the nonbonding $1t_1$ (peak 4 at 5.90 eV) and the average d-band splitting prior to bonding (10.7 − 1.4 = 9.3 eV). It should be noted that this gives a 3d–4s splitting prior to bonding of 8.2 eV, a value which should be independent of ligand type for Zn(II) although it is 1.4–1.8 eV smaller than the optically measured free ion 3d–4s splitting. The results of these calculations are presented in Table IVA, where the average 3d mixing coefficient of 23% O 2p is very close to the values obtained from the Gelius results in Table III and the Xα–SW calculations (Table II).

(2) $ZnCl_4^{2-}$. This analysis is extended to the valence band spectra of $ZnCl_4^{2-}$ given in Figure 6. The energy splittings were taken from the fits of the data, leading to a larger value of the $1a_1$ stabilization (peak 3a) of 2.8 eV (compared with 1.5 eV for ZnO) and a smaller stabilization of the bonding $2t_2$ level (peak 3b) at 1.0 eV relative to the nonbonding peak 4. The greater stabilization of the a_1 level in $ZnCl_4^{2-}$ arises from both a decreased value of Δ relative to that of the oxide ligand and a larger T (Table IVB). The results of the Cl 3p–Zn 3d interaction again reflect the intensity analysis, showing smaller mixing in the d band than for ZnO, ~85% Zn 3d. The smaller amount of ligand p–metal d interaction can be traced to two factors in Table IV, the larger value of Δ and the much smaller T for t_2. Finally, the Zn(II) 3d–4s splitting prior to bonding is determined to be 8.3 eV, consistent with the value obtained from ZnO.

(3) CuCl. For CuCl the 4s/4p stabilized a_1/t_2 levels are assigned as peak 1 in Figure 11, which gives the stabilization of 1.3 eV for each relative to the nonbonding levels of peak 2. We must further realize that the $1t_2$ (s) level is also interacting with the Cu 3d t_2 level, which should stabilize it by about 1.0 eV (from the d-band splitting), leaving only 0.3 eV as the value of x for the 4p stabilization. Values for the respective Δ's were obtained as with the Zn complexes, which gives Δ_{4s-3p} = 6.5 eV and Δ_{4p-3p} = 12.5 eV as the 4s–4p splitting for a Cu^+ ion is ~6 eV.[44] These parameters give $T(a_1)$ = 3.18 and $T(t_2/4p)$ = 1.96, values which display a trend similar to those of $ZnCl_4^{2-}$ but which are significantly smaller. The smaller values of T and larger Δ's both contribute to the reduced 4s/4p mixing in CuCl and hence less covalent bond stabilization.

In analyzing the peak energies of the d band 2e* (peak 3) and $3t_2$* (peak 4) of CuCl, we assume the 2e* level to be nonbonding. This is necessary as the stabilization of the ligand bonding 1e level from the nonbonding $1t_1$ cannot be determined from the spectra. This gives $x(t_2)$ = 1.05 eV with the value of Δ_{3p-3d} taken as the peak 3–peak 2 splitting of 2.8 eV. The results in Table IVC give a t_2 level having 79% Cu 3d character, which is in reasonable agreement with the Gelius analysis, which gave 75% Cu 3d.[61]

(D) Determination of d-Electron Coulomb Repulsion from Resonance PES. As stated earlier, the multielectron satellite in the spectra of the three d^{10} complexes represents a $3d^84s^1$ final state. This assignment results from the resonance enhancement of this feature at the metal 3p → 4s transition energy, as shown in Scheme V. The binding energy difference between the satellite and the d band in the PES spectrum reflects the energy difference between the $3d^84s^1$ and $3d^9$ final states. The ionization of a d^{10} electron to reach a d^9 final state (e_d) is simply the energy difference between the d^{10} and d^9 configurations. The d^{10} configuration energy can be expressed in terms of the potential and kinetic energy of an electron in the field of the nucleus (K) and the two-electron Slater repulsion integrals (F_0, F_2, F_4) as $10K + 45F_0 + 45D$, where $D = -{}^{1}/_{9}F_2 - 14F_4$.[62] Similarly, the d^9 configuration energy is $9K + 36F_0 - 36D$, giving $e_d = E(d^9) - E(d^{10}) = -K - 9F_0 + 9D$.[26,63] The d^9 ionization energy is equal to $E(d^8) - E(d^9) = -K - 8F_0 + 8D$. The energy difference between the d^9 (d band) and $3d^84s^1$ (satellite) final states in the PES spectrum is the difference in the d^{10} and d^9 ionization energies plus the 3d → $2a_1$ transition energy, $-F_0 + D + e_{3d\rightarrow 2a_1}$. The term $-F_0 + D$ is the difference in electron repulsion in the d levels of these two states and is the Coulomb repulsion integral, U, for the d electrons.

Scheme V

$$\text{resonance} \quad 3p^63d^{10} \xrightarrow{\text{ABS}} 3p^53d^{10}4s^1 \xrightarrow{\text{SCK}} 3p^63d^84s^1$$

$$\text{d band ionization} \quad 3p^63d^{10} \rightarrow 3p^63d^9$$

$$\text{shake-up satellite} \quad 3p^63d^{10} \rightarrow 3p^63d^84s^1$$

The satellite–d-band splitting in ZnO is 21.0 eV (Figure 4), and the 3p edge data determine the 3d–4s splitting to be 11.1 eV (see analysis 1), producing U = 9.9 eV. The U value determined for $ZnCl_4^{2-}$ is 10.2 eV, and for CuCl U = 8.5 eV. The larger values for the zinc complexes reflect the greater effective nuclear charge present for this ion, which brings about d orbital contraction and larger electron repulsion. Finally, the U values for these complexes are greatly reduced from the free ion values of 19.7 eV for Zn and 16.5 eV for Cu.[64] These reductions represent changes due

(61) As it is unlikely that the e levels are purely nonbonding, the parameters were modified to reproduce the 25% mixing of the t_2 level of the Gelius analysis; we then obtain Δ = 2.55 eV, $x(t_2)$ = 1.30 eV, and $x(e)$ = 0.25 eV, which give $T(t_2)$ = 2.21 and $T(e)$ = 0.84. The mixing coefficients of the e level of the d band become 92% Cu 3d and 8% Cl 3p, and there is an average mixing of 18% as compared to 15% from the Gelius analysis.

(62) Ferguson, J. *Prog. Inorg. Chem.* **1970**, *12*, 159.

(63) Griffith, J. S. *The Theory of Transition Metal Ions*; Cambridge University Press: London, 1961.

(64) Calculated from ref 41 with the equation $U_{d-d} = E(d^{10}) + E(d^8) - 2E(d^9)$ = 16.5 eV for Cu. To determine the extent of Cu 3d–4s repulsion, this calculation is compared to $E(d^{10}4s^1) + E(d^84s^1) - 2E(3d^94s^1) = U_{d-d} + U_{d-4s}$ = 16.0 eV with the d^84s^1 and d^94s^1 multiplet energies averaged. This implies that metal 3d–4s electron repulsion contributes little, and it has thus been ignored.

to nephelauxetic expansion of the d orbitals through covalent interactions with the ligands and, hence, reflect this covalency.[26] In comparing ZnO to $ZnCl_4^{2-}$, we see a larger reduction in U relative to that of the free ion, consistent with the increased covalency of the oxide d levels as determined from the d-band PES intensities and molecular orbital calculations (Tables III and IV).

V. Discussion

The PES spectral changes produced by the systematic variation of ligand and metal ions reveal important differences in the bonding interactions of d^{10} complexes. The most significant difference in the valence bands of ZnO and $ZnCl_4^{2-}$ is the measurably broader d band of ZnO (Figure 2a,b), which indicates a larger splitting of the t_2 and e d-band components. This variation in splitting shows that a significant change in the ligand field strength, $10Dq$, is associated with chloride versus oxide ligation. It is first important to note that $10Dq$ is inverted for the Zn^{2+} complexes, with the t_2 level appearing to deeper binding energy than the e level in tetrahedral symmetry. This inversion is due to the large effective nuclear charge of the Zn^{2+} ion, which shifts the 3d levels below the ligand levels (Scheme II, left), marking these levels bonding instead of antibonding. The values of $10Dq$ are estimated from the PES spectra to be 6400 cm^{-1} for ZnO and <4000 cm^{-1} for $ZnCl_4^{2-}$; these relative values are consistent with the position of these ligands in the spectrochemical series. The source of the larger $10Dq$ for ZnO is evident in the variable photon energy data in Figure 1, which shows more d character in the destabilized, antibonding ligand levels (peak 5) than observed for $ZnCl_4^{2-}$ in Figure 6. This qualitative behavior and the quantitative intensity and energy splitting analyses indicate that a larger σ-bonding interaction is stabilizing the t_2 level more in ZnO. Greater σ bonding of the oxide ligands is related to both a smaller Δ (i.e. a smaller Zn 3d–O 2p splitting) and large T (i.e. overlap) in the molecular orbital scheme (Table IV).

In a comparison of the spectra of the two chloride salts, the principal differences are the much larger energy stabilizations of the a_1 and t_2 ligand-based bonding levels (peaks 3a and 3b for $ZnCl_4^{2-}$ and peak 2 for CuCl in Figure 8b,d). The larger stabilizations require greater covalent bonding in the Zn^{2+} complex, which derives from two electronic contributions. The greater effective nuclear charge of Zn^{2+} shifts the empty 4s and 4p levels to energies much closer to the ligand levels and thus at a more favorable bonding position than in Cu^+ (for the 3p–4s splitting, Δ = 3.7 eV for Zn^{2+} and 6.5 eV for Cu^+). From Table IV, large increases in T for the Zn 4s/4p–Cl 3p interactions relative to those for Cu^+ also contribute, which are not simply derived from overlap effects as the 4s and 4p orbitals of the more high charged Zn^{2+} ion must be more contracted than those of Cu^+, and the bond lengths are quite similar (2.25 Å[29] for $ZnCl_4^{2-}$ and 2.34 Å for CuCl).

Zn^{2+} complexes with donor ligands are much more stable thermodynamically than their Cu^+ counterparts as demonstrated by the substantially larger heats of formation of the Zn^{2+} systems.[65] Specifically, $ZnCl_2$(s) has ΔH_f° = −99.4 kcal/mol while ΔH_f° = −32.5 kcal/mol for CuCl(s), a trend which continues for all such comparable materials. In addition, Zn^{2+} ions have much larger heats of solvation than Cu^+, which is illustrated in the ΔH_{solv} value for each in DMSO: −506 kcal/mol for Zn^{2+} and −155 kcal/mol for Cu^+.[66] While the larger charge on the Zn^{2+} ion and its resulting smaller radius will obviously lead to greater Coulombic effects, the PES results summarized above indicate that greater covalent bonding in the Zn^{2+} complexes should also contribute to their enhanced stability.

It has been noted by several authors[67-69] that for many extended-lattice transition-metal complexes, the lattice energies calculated with the Born–Haber cycle exceed the lattice energies determined from simple electrostatic (Madelung-type) calculations. This difference has often been attributed to crystal field stabilization energies (CFSE) of the partially filled d levels.[68] Waddington[67] observed, however, that these lattice energy discrepancies do not closely follow the CFSE trends. In fact, a different trend related to the covalency of the complexes is present. For example, the differences between the Born–Haber and electrostatic calculations for CoF_2, $CoBr_2$, and CoI_2 are −20, −88 and −103 kcal/mol, respectively, while the CFSE values are only −24.8, −20, and −26.5 kcal/mol.[67] Thus, an additional energy term related to the covalent energy stabilization ($\Delta H_{covalent}$) should be included in the Born–Haber calculation:

$$\Delta H_f^\circ = a\Delta H_A^M + b\Delta H_A^L + aIP^M + bEA^L + \Delta H_{ionic} + \Delta H_{covalent} - nRT \quad (7)$$

In this equation, ΔH_f° is the heat of formation of the solid M_aL_b, ΔH_A is the heat of atomization of the metal (M) or ligand (L), IP^M is the sum of the ionization potentials to form the metal ion, EA^L is the total electron affinity to form the ligand anion, and ΔH_{ionic} is the electrostatic lattice energy, which can be approximated by the Born–Lande equation:[70]

$$\Delta H_{ionic} = \frac{NAz_Mz_Le^2}{r}\left(1 - \frac{1}{n}\right) \quad (8)$$

In eq 8, N is Avogadro's number, A is the Madelung constant for the crystalline lattice, z is the charge on the metal (M) or ligand (L) ion, e is the fundamental charge unit, r is the shortest M–L distance, and n is the Born exponent. The term $1 - 1/n$ approximates the repulsive interactions occurring, and n can be determined from compressibility data.[69,71,72]

To use this analysis for d^{10} complexes, the thermodynamic values for CuCl are compared to those of $ZnCl_2$. $ZnCl_2$ has an extended-lattice structure to allow calculation of ΔH_{ionic}, and its thermodynamic properties are well-known. In addition, $ZnCl_2$ contains tetrahedrally coordinated Zn^{2+} ions[73] and its PES spectrum[74] is quite similar to that of $ZnCl_4^{2-}$. The values used in the Born–Haber calculations are presented in Table V, along with the calculated ΔH_{ionic} value; $\Delta H_{covalent}$ is calculated as the difference between the Born–Haber lattice energy and the electrostatic lattice energy. A subatantially larger negative $\Delta H_{covalent}$ is obtained for $ZnCl_2$ (−69 kcal/mol) than for CuCl (−26 kcal/mol), indicating larger covalent energy stabilization for $ZnCl_2$. (As an aside, d^{10} complexes can obviously have no CFSE, so $\Delta H_{covalent}$ clearly cannot be attributed to this CFSE.) For comparison, Waddington[67] has determined $\Delta H_{covalent}$ = −22 kcal/mol for ZnF_2, a value that is logically much less than we determine for the more covalent $ZnCl_2$.

Table V. Thermodynamic Quantities (kcal/mol)[a]

estimate	ΔH_f	ΔH_{ionic}	ΔH_{M^+}	ΔH_{L^-}	ΔH_{cov}	PES
$ZnCl_2$	−99.4	−580	660	−108	−69.4	−133
CuCl	−32.5	−210	259	−54.2	−26.0	−25

[a] The values of ΔH_{M^+} and ΔH_{L^-} include both the heats of atomization and ionization potentials or electron affinities as in eq 7. The value of n in eq 8 is 10.5, taken from ref 72.

There is consistency in both the PES and thermodynamic data requiring that $ZnCl_2$ have more covalent bond energy than CuCl. For both $ZnCl_2$ and CuCl, however, covalent bonding accounts for only about 10% of the total energy stabilization of the complex from the free ions. As a first approximation to this covalent energy, the energy stabilizations of the bonding a_1 and t_2 levels relative to the nonbonding t_1 position obtained from the PES data were weighted by the total number of electrons in each level

(65) For a compilation of ΔH_f°, see: *CRC Handbook of Chemistry and Physics*, 64th ed.; Weast, R. C., Ed.; Chemical Rubber Company: Boca Raton, FL, 1983.
(66) Ahrland, S. *Pure Appl. Chem.* **1982**, *54*, 1451.
(67) Waddington, T. C. *Adv. Inorg. Chem. Radiochem.* **1959**, *1*, 157.
(68) Ladd, M. F. C.; Lee, W. H. *Prog. Solid State Chem.* **1961**, *1*, 37.
(69) Tosi, M. P. *Solid State Phys.* **1964**, *16*, 1.
(70) Born, M.; Lande, A. *Sitzungsber. Preuss, Akad. Wiss., Phys.-Math. Kl., Berlin* **1918**, *45*, 1048.
(71) Born, M.; Mayer, J. E. *Z. Phys.* **1932**, *75*, 1.
(72) Mayer, J. E.; Levy, R. B. *J. Chem. Phys.* **1933**, *1*, 647.
(73) Byrnestad, J.; Yakel, H. L. *Inorg. Chem.* **1978**, *17*, 1376.
(74) Pong, W.; Okada, S. K. *Phys. Rev. B: Condens. Matter* **1979**, *19*, 5307.

stabilized per mole. This calculation leads to the values in the final column of Table V, −133 kcal/mol for $ZnCl_2$ and −25 kcal/mol for CuCl, a trend which agrees with the thermodynamic data. The agreement for $ZnCl_2$ is, of course, far from quantitative, which emphasizes that valence band energy stabilizations are only one important contribution to the total energy changes occurring upon covalent bonding.

Thus, Zn^{2+} complexes with σ-donor, π-donor ligands have large ionic and substantial covalent contributions to the chemical bonds. Both the ionic and covalent terms should be much smaller in the case of Cu^+. In particular, the low effective nuclear charge on Cu^+ together with the filled d levels and limited charge donation lead to weak bonding with donor ligands. The very low binding energy of the Cu^+ d^{10} levels, however, should make them readily accessible to back-bonding with π-acceptor ligands and lead to much stronger covalent interactions. In this regard, Cu^+ complexes with sulfur or CO ligands are, in fact, much more stable than the analogous Zn^{2+} complexes. Finally, we note that the low binding energies of Cu^+ d levels also lead to clear energy separation from the ligand levels, allowing the unobscured study of the d manifold, a fact which could have important implications in the PES study of the Cu(I)/Cu(II) redox couple.

Acknowledgment. We thank Dr. Andrew A. Gewirth for the SCF–Xα–SW calculation on $CuCl_4^{3-}$ and Professor T. Geballe for the gift of a CuCl sample. We acknowledge financial support of this research by the donors of the Petroleum Research Fund, administered by the American Chemical Society. The Stanford Synchrotron Radiation Laboratory, which is supported by the U.S. Department of Energy, has provided beam time, and the Stanford Center for Materials Research, supported by the Materials Research Division of the National Science Foundation, has provided experimental facilities for this research.

Registry No. ZnO, 1314-13-2; CuCl, 7758-89-6; $ZnCl_4^{2-}$, 15201-05-5.

Contribution from the Department of Chemistry,
Texas A&M University, College Station, Texas 77843-3255

Electronic Structure of Metal Clusters. 6. Photoelectron Spectra and Molecular Orbital Calculations of Bis(μ_3-sulfido)- and Bis(μ_3-selenido)nonacarbonyltriosmium

Greg L. Griewe and Michael B. Hall*

Received June 22, 1987

Gas-phase, ultraviolet photoelectron (PE) spectra and molecular orbital (MO) calculations are reported for $Os_3(CO)_9(\mu_3\text{-}X)_2$ (X = S, Se). The spectra are similar to that reported for $Fe_3(CO)_9(\mu_3\text{-}S)_2$ but have increased band definition. The HOMO, a 3c-2e (Os–Os–Os) bond, is dominated by the e_g-like orbitals of the $Os(CO)_3$ fragment and contains most of the net metal–metal overlap population. Ionization from this orbital occurs at lower energy than the remaining ionizations. The t_{2g}-like orbitals on the $Os(CO)_3$ fragments make little or no net contribution to Os–X or to Os–Os bonding. The e_g-like and, to a lesser extent, the a_1-like orbitals on the metal fragments are responsible for nearly all of the Os–Os and Os–X (X = S, Se) bonds in the cluster.

Introduction

Metal clusters with bridging chalcogens are an important class of compounds. Chalcogens possess a wide range of possible coordination numbers and form relatively strong bonds to transition metals.[1] Triply bridging chalcogens contain a lone pair of electrons that can bond to unsaturated metal fragments[2] or to small clusters,[3] forming higher nuclearity clusters. They can also provide a convenient route to the preparation of mixed-metal clusters.[4] Several theoretical papers have appeared on $Fe_3(CO)_9(\mu_3\text{-}S)_2$,[5] which can be considered a model for more complicated systems. Rives et al.[5a] used Fenske–Hall molecular orbital calculations[6] to evaluate the bonding in an idealized model of $Fe_3(CO)_9S_2$ with 3-fold symmetry. They also used an empirical orbital localization procedure to determine which orbitals were bonds and which were lone pairs. Chesky et al.[5b] used Fenske–Hall calculations and He I photoelectron (PE) spectra to evaluate the bonding in $Fe_3(CO)_9S_2$ and related compounds with triply bridging sulfidos. The He II PE spectra have also been reported.[5c] The spectra in both papers consisted of two broad and relatively featureless groups of bands that were not amenable to detailed evaluation or comparison with the calculations.

This study will examine the bonding in $Os_3(CO)_9(\mu_3\text{-}X)_2$ (X = S, Se) using gas-phase, ultraviolet He I PE spectroscopy. The PE spectra will be interpreted by observing trends and comparing the spectra with parameter-free molecular orbital calculations. It is widely accepted that the spectra of second- and third-row homologues of first-row metal compounds have increased band definition due to spin–orbit coupling, kinematic effects of the heavier metal on the band envelope, and larger photoionization cross sections of 4d and 5d orbitals.[7] With enhanced definition of the PE spectra, comparison with the theoretical calculations should yield a more detailed understanding of the bonding in this class of clusters.

Experimental Section

$Os_3(CO)_9(\mu\text{-}S)_2$ and $Os_3(CO)_9(\mu_3\text{-}Se)_2$ were prepared according to a published procedure.[8] The ultraviolet photoelectron spectra were recorded on a Perkin-Elmer Model PS-18 spectrometer. The total spectra were recorded as single slow scans with the argon $^2P_{3/2}$ and $^2P_{1/2}$ lines at 15.76 and 15.94 eV, respectively, used as the internal reference. No free CO spike at 14 eV was observed, indicating that both compounds were stable and did not decompose in the spectrometer. The resolution for all spectra was better than 40 meV for the fwhm of the argon $^2P_{3/2}$ peak.

(1) (a) Adams, R. D.; Horvath, I. T.; Mathur, P.; Segmueller, B. E.; Yang, L. W. *Organometallics* **1983**, *2*, 1078. (b) Vahrenkamp, H. *Angew. Chem., Int. Ed. Engl.* **1975**, *14*, 322.
(2) (a) Adams, R. D. *Polyhedron* **1975**, *4*, 2003. (b) Adams, R. D.; Männing, D.; Segmueller, B. E. *Organometallics* **1983**, *2*, 149. (c) Winter, A.; Jibril, I.; Huttner, G. *J. Organomet. Chem.* **1983**, *242*, 259. (d) Seyferth, D.; Henderson, R. S.; Fackler, J. P., Jr.; Mazany, A. M. *J. Organomet. Chem.* **1981**, *213*, C21. (e) Richter, F.; Vahrenkamp, H. *Angew. Chem., Int. Ed. Engl.* **1978**, *17*, 444.
(3) (a) Adams, R. D.; Dawoodi, Z.; Foust, D. *Organometallics* **1982**, *1*, 411. (b) Adams, R. D.; Horvath, I. T.; Wang, L. W. *J. Am. Chem. Soc.* **1983**, *105*, 1533.
(4) (a) Adams, R. D.; Horvath, I. T.; Wang, S. *Inorg. Chem.* **1986**, *25*, 1617. (b) Adams, R. D.; Horvath, I. T.; Mathur, P. J. *J. Am. Chem. Soc.* **1983**, *105*, 7202. (c) Adams, R. D.; Horvath, I. T.; Segmueller, B. E.; Yang, L. W. *Organometallics* **1983**, *2*, 1301. (d) Adams, R. D.; Hor, T. S. A.; Horvath, I. T. *Inorg. Chem.* **1984**, *23*, 4733.
(5) (a) Rives, A. B.; Xiao-Zeng, Y.; Fenske, R. F. *Inorg. Chem.* **1982**, *21*, 2286. (b) Chesky, P. T.; Hall, M. B. *Inorg. Chem.* **1983**, *22*, 2998. (c) Van Dam, H.; Stufkens, D. J.; Oskam, A. *Inorg. Chim. Acta* **1978**, *31*, L377.
(6) Hall, M. B.; Fenske, R. F. *Inorg. Chem.* **1972**, *11*, 768.
(7) Higginson, B. K.; Lloyd, D. R.; Burroughs, P.; Gibson, D. M.; Orchard, A. F. *J. Chem. Soc., Faraday Trans. 2* **1973**, *69*, 1659.
(8) Johnson, B. F. G.; Lewis, J.; Raithby, P. R.; Hendrick, K.; McPartlin, M. *J. Chem. Soc., Chem. Commun.* **1979**, *16*, 719.

0020-1669/88/1327-2250$01.50/0